Field-angle Resolved Flux-flow Resistivity as a Phase-sensitive Probe of Unconventional Cooper Pairing

Yoichi Higashi[1,3], Yuki Nagai[2], Masahiko Machida[2], and Nobuhiko Hayashi[3]
[1]*Department of Mathematical Sciences, Osaka Prefecture University, 1-1 Gakuen-cho, Naka-ku, Sakai 599-8531, Japan*
[2]*CCSE, Japan Atomic Energy Agency, 5-1-5 Kashiwanoha, Kashiwa, Chiba 277-8587, Japan*
[3]*Nanoscience and Nanotechnology Research Center (N2RC), Osaka Prefecture University, 1-2 Gakuen-cho, Naka-ku, Sakai 599-8570, Japan*

(Dated: April 25, 2013)

We theoretically investigate the applied magnetic field-angle dependence of the flux-flow resistivity $\rho_{\rm f}(\alpha_{\rm M})$ for an uniaxially anisotropic Fermi surface. $\rho_{\rm f}$ is related to the quasiparticle scattering rate Γ inside a vortex core, which reflects the sign change in the superconducting pair potential. We find that $\rho_{\rm f}(\alpha_{\rm M})$ is sensitive to the sign-change in the pair potential and has its maximum when the magnetic field is parallel to the gap-node direction. We propose the measurement of the field-angle dependent oscillation of $\rho_{\rm f}(\alpha_{\rm M})$ as a phase-sensitive field-angle resolved experiment.

PACS numbers: 74.20.Rp, 74.25.Op, 74.25.nn,

To elucidate the symmetry of superconducting pair potential is of great importance for studying Cooper pairing mechanism in unconventional superconductors (SCs). The pair potential is composed of spin and orbital wave functions. The orbital wave function is characterized by its amplitude and phase (sign of wave function).

In the last decade, experimental techniques for the field-angle resolved specific heat and thermal conductivity measurements have developed to identify the Cooper pairing symmetry in various superconducting systems [1]. These angle-resolved mesurements are powerful techniques that can detect the anisotropy of the pair potential amplitude. However, they cannot probe the sign change in the pair potential. That is, these angle-resolved measurements are not phase-sensitive probes. In addition to detecting the anisotropy of the pair potential, it is crucial to probe the phase of the Cooper pair in order to discriminate unconventional SCs including iron-based SCs from conventional one.

Until now, only a few phase-sensitive probes have been developed, for example the half-flux quantum observation in the tricrystal geometry by scanning SQUID (superconducting quantum interference device) microscope [2] and detecting the quasiparticle interference pattern by scanning tunneling spectroscopy [3]. In addition to these existing experiments, a new phase-sensitive test is highly desired.

In this paper, we propose a new phase-sensitive experiment. we theoretically study the in-plane field-angle dependence of the flux-flow resistivity $\rho_{\rm f}(\alpha_{\rm M})$ for typical gap functions and Fermi surface (FS). From our numerical calculations, we show that the phase-sensitive QP scattering inside a vortex core leads to differnt behavior of $\rho_{\rm f}(\alpha_{\rm M})$ between conventional and unconventional Cooper pairing. In addition, we show that $\rho_{\rm f}(\alpha_{\rm M})$ has its maximum when the applied magnetic field is parallel to gap-node directions. Our results show that the field-angle dependence of the flux-flow resistivity can detect both the sign change of pair potential and the direction of gap nodes.

The flux-flow resistivity $\rho_{\rm f}$ is dominated by the quasiparticle within a vortex core. There are two important contributions to $\rho_{\rm f}$. One is the QP scattering rate Γ inside a vortex core and the other is the momentum dependent quantum level spacing of the vortex bound states $\omega_0(\boldsymbol{k}_{\rm F})$ [4]. Here, the QP scattering is due to nonmagnetic impurities randomly distributed in the system.

We attribute the flux-flow resistivity $\rho_{\rm f}$ to the energy dissipation of the vortex bound states due to the impurity scattering inside a vortex core [5]. $\rho_{\rm f}$ is characterized by the two quantities mentioned above [4],

$$\rho_{\rm f}(T) \propto \frac{\Gamma_{\rm n}}{\Delta_\infty}\left[\frac{1}{\nu_0}\int \frac{dS_{\rm F}}{|\boldsymbol{v}_{\rm F}(\boldsymbol{k}_{\rm F})|}\frac{\omega_0(\boldsymbol{k}_{\rm F})}{\Delta_\infty}\frac{\Gamma_{\rm n}}{\Gamma(\varepsilon=k_{\rm B}T,\boldsymbol{k}_{\rm F})}\right]^{-1}, \tag{1}$$

where $\Gamma_{\rm n}$ is the scattering rate in the normal state. We have assumed the moderately clean regime [5]. We assume that the temperature T dependence of $\rho_{\rm f}$ is predominantly comes from Γ with the QP energy $\varepsilon = k_{\rm B}T$. Here, we have made the rough estimate. Actually the QPs distributed with the energy width $\Delta\varepsilon \sim k_{\rm B}T$ contribute to Γ. The total density of states on a FS is $\nu_0 = \int dS_{\rm F}/|\boldsymbol{v}_{\rm F}(\boldsymbol{k}_{\rm F})|$ with $dS_{\rm F} = |\boldsymbol{k}_{\rm F}(\phi_k,\theta_k)|^2 \sin\theta_k d\phi_k d\theta_k$ being an area element on the FS, the Fermi velocity $\boldsymbol{v}_{\rm F}(\boldsymbol{k}_{\rm F}) = \boldsymbol{\nabla}_{\boldsymbol{k}}\epsilon(\boldsymbol{k})|_{\boldsymbol{k}=\boldsymbol{k}_{\rm F}}$ and the Fermi wave vector $\boldsymbol{k}_{\rm F} = |\boldsymbol{k}_{\rm F}(\phi_k,\theta_k)|(\bar{\boldsymbol{a}}\cos\phi_k\sin\theta_k + \bar{\boldsymbol{b}}\sin\phi_k\sin\theta_k + \bar{\boldsymbol{c}}\cos\theta_k)$. $\epsilon(\boldsymbol{k})$ is the energy dispersion of electrons. ϕ_k (θ_k) is the azimuthal (polar) angle on the FS. $\bar{\boldsymbol{a}}$, $\bar{\boldsymbol{b}}$ and $\bar{\boldsymbol{c}}$ denote orthogonal unit vectors spanning crystal coordinates. We use the unit system in which $\hbar = 1$.

The momentum dependent inter-level spacing of the vortex bound states $\omega_0(\boldsymbol{k}_{\rm F})$ is obtained analytically as [6, 7] $\omega_0(\boldsymbol{k}_{\rm F}) = 2|d(\boldsymbol{k}_{\rm F})|^2\Delta_\infty^2/(|\boldsymbol{k}_{\rm F\perp}||\boldsymbol{v}_{\rm F\perp}(\boldsymbol{k}_{\rm F})|)$ using the quasiclassical Green's function method and the Kramer-Pesch approximation [8, 9]. We treat the non-magnetic impurity scattering by means of the Born approximation [10]. The quasiparticle scattering rate for the QPs with the energy ε inside a vortex core is obtained as [9, 11]

$$\frac{\Gamma(\varepsilon)}{\Gamma_{\rm n}} = \left\langle \left\langle \frac{\Gamma(\boldsymbol{k}_{\rm F}, \boldsymbol{k}'_{\rm F}, \varepsilon)}{\Gamma_{\rm n}} \right\rangle_{\rm FS'} \right\rangle_{\rm FS}, \tag{2}$$

$$\frac{\Gamma(\boldsymbol{k}_{\rm F}, \boldsymbol{k}'_{\rm F}, \varepsilon)}{\Gamma_{\rm n}} = \frac{\pi}{2} C(\boldsymbol{k}_{\rm F}, \boldsymbol{k}'_{\rm F}) D(\boldsymbol{k}_{\rm F}, \boldsymbol{k}'_{\rm F}) F(\varepsilon, \boldsymbol{k}_{\rm F}, \boldsymbol{k}'_{\rm F}), \tag{3}$$

$$C(\boldsymbol{k}_{\rm F}, \boldsymbol{k}'_{\rm F}) = 1 - {\rm sgn}[d(\boldsymbol{k}_{\rm F}) d(\boldsymbol{k}'_{\rm F})] \cos\Theta, \tag{4}$$

$$D(\boldsymbol{k}_{\rm F}, \boldsymbol{k}'_{\rm F}) = \frac{1}{|\sin\Theta|}, \tag{5}$$

$$F(\varepsilon, \boldsymbol{k}_{\rm F}, \boldsymbol{k}'_{\rm F}) = \frac{|\boldsymbol{v}_{\rm F\perp}(\boldsymbol{k}'_{\rm F})|}{|\boldsymbol{v}_{\rm F\perp}(\boldsymbol{k}_{\rm F})|} \frac{|d(\boldsymbol{k}_{\rm F})|}{|d(\boldsymbol{k}'_{\rm F})|} e^{-u(s_0, \boldsymbol{k}_{\rm F})} e^{-u(s'_0, \boldsymbol{k}'_{\rm F})}. \tag{6}$$

Here, $\langle \cdots \rangle \equiv (1/\nu_0) \int dS_{\rm F} \cdots / |\boldsymbol{v}_{\rm F}(\boldsymbol{k}_{\rm F})|$, $\Theta(\boldsymbol{k}_{\rm F}, \boldsymbol{k}'_{\rm F}) \equiv \theta_v(\boldsymbol{k}_{\rm F}) - \theta_{v'}(\boldsymbol{k}'_{\rm F})$ is the scattering angle [see Fig. 1]. Γ has the decay factor $\exp[-u(s_0, \boldsymbol{k}_{\rm F})]$ with $u(s_0, \boldsymbol{k}_{\rm F}) = (2|d(\boldsymbol{k}_{\rm F})|/|\boldsymbol{v}_{\rm F\perp}(\boldsymbol{k}_{\rm F})|) \int_0^{|s_0|} ds' \tilde{\Delta}(s')$. Fig. 1 shows the quasiparticle trajectories on the plane perpendicular to the magnetic field $\boldsymbol{H}$. The quantities with prime are those after scattering. We adopt $\tilde{\Delta}(s') = \Delta_\infty \tanh(s'/\xi_0)$ as the spatial variation of the pair potential. s_0 and $|s'_0|$ denote the length between the point which is the nearest from the vortex core on the QP trajectory and the scattering point [9, 11].

In this study, we consider the case that $\boldsymbol{H}$ is applied parallel to the $a-b$ plane and rotated. The field angle measured from a axis is $\alpha_{\rm M}$. Here, a, b and c are crystal axes. When calculating the dependence of $\rho_{\rm f}$ on the magnetic field angle $\alpha_{\rm M}$, we need a coordinate system fixed to $\boldsymbol{H}$ which is spanned by $\bar{\boldsymbol{a}}_{\rm M}$, $\bar{\boldsymbol{b}}_{\rm M}$, and $\bar{\boldsymbol{c}}_{\rm M}$ (vortex coordinate ststem). Here, these axes are orthogonal unit vectors with $\bar{\boldsymbol{c}}_{\rm M}$ set parallel to $\boldsymbol{H}$ ($\bar{\boldsymbol{c}}_{\rm M} \parallel \boldsymbol{H}$). $\boldsymbol{v}_{\rm F\perp}$, θ_v and those with prime are defined in the vortex coordinates. However, $\boldsymbol{k}_{\rm F}$ and $\boldsymbol{k}'_{\rm F}$ are identified by (ϕ_k, θ_k) on a FS in the crystal coordinates spanned by $\bar{\boldsymbol{a}}$, $\bar{\boldsymbol{b}}$ and $\bar{\boldsymbol{c}}$, which characterize the crystal axes. In order to calculate the field-angle $\alpha_{\rm M}$ dependence of $\rho_{\rm f}$, we need to derive the relation between $\boldsymbol{v}_{\rm F\perp}$, θ_v and $\boldsymbol{v}_{\rm F}$, θ_k [11]. Then, the component of $\boldsymbol{v}_{\rm F}(\boldsymbol{k}_{\rm F})$ projected onto the plane perpendicular to $\boldsymbol{H}$ is finally obtained as

$$|\boldsymbol{v}_{\rm F\perp}(\phi_k, \theta_k)| = |\boldsymbol{v}_{\rm F}(\phi_k, \theta_k)| \Omega(\phi_k, \theta_k), \tag{7}$$

$$\Omega(\phi_k, \theta_k) = \sqrt{\cos^2\theta_k + \sin^2(\phi_k - \alpha_{\rm M}) \sin^2\theta_k}, \tag{8}$$

$$\cos\theta_v(\phi_k, \theta_k) = \frac{-|\boldsymbol{v}_{\rm F}(\phi_k, \theta_k)|}{|\boldsymbol{v}_{\rm F\perp}(\phi_k, \theta_k)|} \cos\theta_k, \tag{9}$$

$$\sin\theta_v(\phi_k, \theta_k) = \frac{|\boldsymbol{v}_{\rm F}(\phi_k, \theta_k)|}{|\boldsymbol{v}_{\rm F\perp}(\phi_k, \theta_k)|} \sin(\phi_k - \alpha_{\rm M}) \sin\theta_k, \tag{10}$$

Thus, the relation between the vortex coordinate and the crystal coordinate is derived. We have now reached to the position where we can perform the numerical integration on FS and calculate the field-angle dependence of Eq. (1).

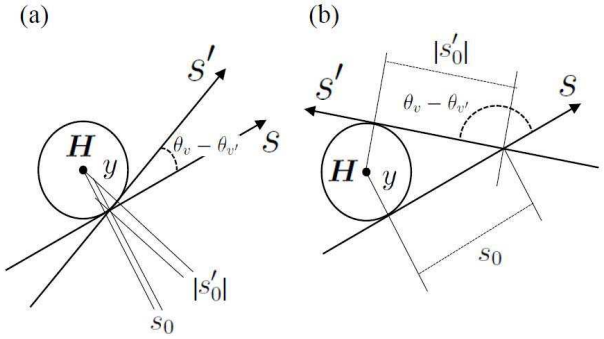

FIG. 1: The schematic figure of (a) the forward scattering and (b) the backward scattering in the vicinity of a vortex. s and s' indicate the QP trajectory before and after scattering, respectively.

We consider the following two types of the simple pair potential model. One is line-node s-wave pair: $d(\boldsymbol{k}_{\rm F}) = |\cos 2\phi_k| \sin^2\theta_k$. The other is $d_{x^2-y^2}$-wave one: $d(\boldsymbol{k}_{\rm F}) = \cos 2\phi_k \sin^2\theta_k$. Each one has gap nodes from the north pole of the FS to the south one in the $\phi_k = (1+2n)\pi/4$ [rad] directions (gap-node directions) with $n = 0, 1, 2, 3$. $\phi_k = n\pi/2$ [rad] directions correspond to anti-node directions. In the momentum space, these two pair potentials have the same anisotropy in their amplitude $|d(\boldsymbol{k}_{\rm F})|$. However, only the d-wave pair has the sign change and the s-wave pair does not.

Our calculations are performed for an uniaxially anisotropic FS with the anisotropy parameter $\gamma = \sqrt{m_c/m_{ab}}$ [12]. m_c and m_{ab} are masses characterizing charge transport along the c-axis and within the $a-b$ plane, respectively.

We show numerical results for an uniaxially anisotropic FS with $\gamma = 3$. In Fig. 2, we show the field-angle dependence of the flux-flow resistivity $\rho_{\rm f}(\alpha_{\rm M})$ for the above pair potential models. As shown in Fig. 2(a), in the case of the line-node s-wave pair, a broad maximum appears when $\boldsymbol{H}$ is applied parallel to the gap-node direction ($\alpha_{\rm M} = \pi/4$). Note that the field-angle dependence of the QP scattering rate $\Gamma(\alpha_{\rm M})$ has its minimum when $\boldsymbol{H}$ is parallel to the node direction [11]. The oscillation amplitude of $\rho_{\rm f}(\alpha_{\rm M})$ remains small compared with the d-wave case when the temperature T is increased. $\rho_{\rm f}(\alpha_{\rm M})$ has little dependence on T in the case of the line-node s-wave pair.

On the other hand, in the d-wave case [Fig. 2(b)], a sharp maximum appears when $\boldsymbol{H}$ is applied to the gap-node direction. The oscillation amplitude grows with increasing T in contrast to the line-node s-wave pair. This behavior indicates that the peak of $\rho_{\rm f}(\alpha_{\rm M})$ has a strong temperature dependence in the d-wave case.

The field-angle dependece of $\rho_{\rm f}$ is quite contrasting be-

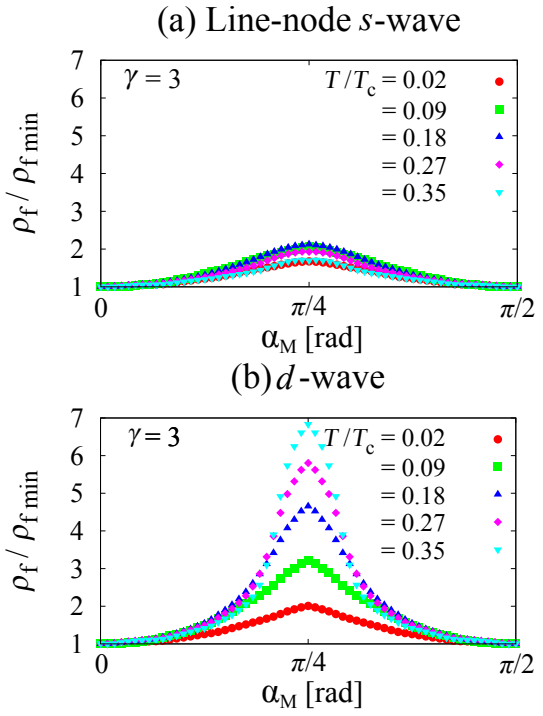

FIG. 2: (Color online) Field-angle ($\alpha_{\rm M}$) dependence of the flux-flow resistivity $\rho_{\rm f}$ in the case of (a) line-node s-wave and (b) d-wave pair for a spheroidal FS ($\gamma = 3$). Each curve indicates different temperature. The vertical axis is normalized by the minimum value of $\rho_{\rm f\ min}$ for each plot.

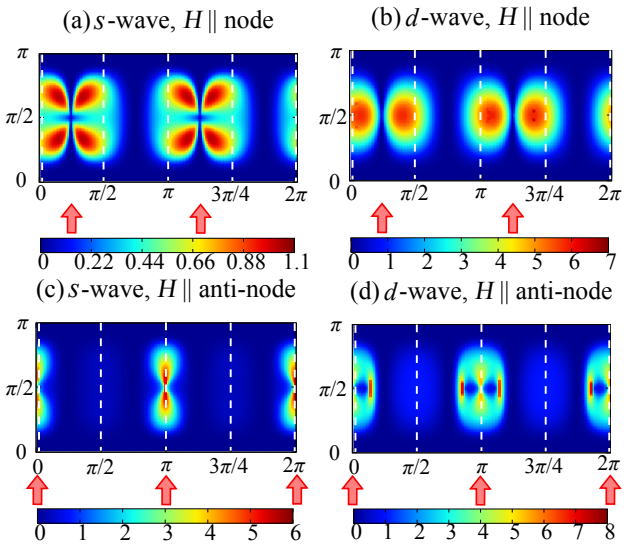

FIG. 3: (Color online) $\boldsymbol{k}_{\rm F}$ dependence of Γ in the case of (a) the line-node s-wave pair when $\boldsymbol{H}$ || the gap-node direction, (b) d-wave pair when $\boldsymbol{H}$ || the gap-node direction, (c) the line-node s-wave pair when $\boldsymbol{H}$ || the anti-node direction and (d) d-wave pair when $\boldsymbol{H}$ || the anti-node direction on a spheroidal FS ($\gamma = 3$). The quasiparticle energy ε is set to $0.2\Delta_0$ in each plot. The vertical and horizontal axes denote the polar angle θ_k and the azimuthal angle ϕ_k respectively. The dotted lines indicate the anit-node directions. The field directions are indicated by arrows.

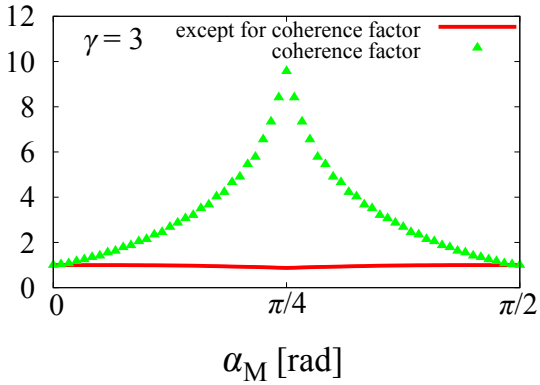

FIG. 4: (Color online) Field-angle ($\alpha_{\rm M}$) dependences of the part of Γ containing the coherence factor and the other part of it for d-wave pair with the spheroidal FS. The vertical axis is normalized by the minimum value.

tween the line-node s-wave pair and the d-wave one. One would question what the reason of this prominent difference is. We consider that this difference comes from whether there is the sign change in the pair potential or not.

At first, we list the characteristics of $\Gamma(\boldsymbol{k}_{\rm F})/\Gamma_{\rm n}$. $\Gamma(\boldsymbol{k}_{\rm F})/\Gamma_{\rm n}$ is obtained by integrating Eq. (3) with respect to $\boldsymbol{k}'_{\rm F}$. Next, we explain the behavior of $\Gamma(\alpha_{\rm M})$.

In order to clarify why $\rho_{\rm f}(\alpha_{\rm M})$ behaves contrastingly between these pair potential models, we investigate the $\boldsymbol{k}_{\rm F}$ dependence of Γ first. $\Gamma(\boldsymbol{k}_{\rm F})/\Gamma_{\rm n}$ indicates which QPs are easy to be scattered on the FS. We find the following characteristics of the QP scattering (i) – (iii). (i) The QPs in the vicinity of the anti-node direction predominantly contribute to Γ as seen in Figs. 3(a)–(d). $\Gamma(\boldsymbol{k}_{\rm F})/\Gamma_{\rm n}$ has higher value around around anti-node directions (see around dotted lines). (ii) There is the tendency that the QPs in the direction of $\boldsymbol{H}$ are easy to be scattered. As seen in Figs. 3(a) and 3(b), this property of the QP scattering is confirmed by the fact that the weight of Γ shifts a bit toward the field direction. The tendency is obvious in Figs. 3(c) and 3(d). The reason why QPs have above tendency is because $|\boldsymbol{v}_{\rm F\perp}(\boldsymbol{k}_{\rm F})|$ of QPs in the field direction is small and the contribution to Γ becomes large [see Eq. (6)]. (iii) The other contribution to Γ is expressed by the coherence factor $C(\boldsymbol{k}_{\rm F}, \boldsymbol{k}'_{\rm F})$ [9], which reflects the sign of the pair potential in Eq. (4). This characteristic is discussed in detail in Ref. [9]. Here we summarize their results in Table I.

First of all, we consider Γ, which is a part of the contribution to $\rho_{\rm f}$. In the case of the line-node s-wave pair, taking into account the characteristics of the QP scattering (i) – (iii), we can explain qualitatively the behavior of $\rho_{\rm f}(\alpha_{\rm M})$. In the s-wave pair, $\Gamma(\alpha_{\rm M})$ has its minimum

TABLE I: The QP scattering types.

	forward scattering	backward scattering
sign-conserved	suppressed	small
sign-reversed	enhanced	suppressed

when $\boldsymbol{H}$ is applied to the gap-node direction [11]. In this case, according to the factor (iii), the effect of the coherence factor on $\Gamma(\boldsymbol{k}_{\rm F})/\Gamma_{\rm n}$ is small. In addition, in the line-node s-wave pair, we confirmed that the coherence factor has no field-angle dependence. Hence, we can neglect the factor (iii) in the s-wave pair. When $\boldsymbol{H}$ is parallel to the gap-node direction, the weight of $\Gamma(\boldsymbol{k}_{\rm F})/\Gamma_{\rm n}$ shift toward the field direction (i.e., gap-node direction) due to the factor (ii). Therefore, the QPs around the gap node get easier to be scattered. However, according to the factor (i), the contribution of the QPs in the vicinity of the gap nodes to $\Gamma(\boldsymbol{k}_{\rm F})/\Gamma_{\rm n}$ is small. Hence, the large contribution to $\Gamma(\boldsymbol{k}_{\rm F})/\Gamma_{\rm n}$ due to the factor (ii) gets small due to the factor (i).

On the other hand, when $\boldsymbol{H}$ is parallel to the anti-node direction, the QPs in the direction of $\boldsymbol{H}$ (i.e., anti-node direction) ,which have small $\boldsymbol{v}_{\rm F\perp}(\boldsymbol{k}_{\rm F})$, can give a large contribution to $\Gamma(\boldsymbol{k}_{\rm F})/\Gamma_{\rm n}$ due to the factor (ii). In this case, differently from the case of $\boldsymbol{H}$ || the node direction, Γ remains large due to the factor (i). As a result of the above consideration, the minimum of $\Gamma(\alpha_{\rm M})$ appears when $\boldsymbol{H}$ is parallel to the gap-node direction.

In the case of d-wave pair, the backward scattering is suppressed [see Table I] since the coherence factor becomes zero and the scattering point is far from the vortex core. However, the forward scattering with the sign-change of pair potential is enhanced [Table I] so that the coherence factor gives the large contribution to $\Gamma(\boldsymbol{k}_{\rm F})/\Gamma_{\rm n}$. In Fig. 4, we show the field-angle dependences of $\langle\langle C(\boldsymbol{k}_{\rm F},\boldsymbol{k}'_{\rm F})D(\boldsymbol{k}_{\rm F},\boldsymbol{k}'_{\rm F})\rangle_{\rm FS'}\rangle_{\rm FS}$, which is the part of $\Gamma(\varepsilon)/\Gamma_{\rm n}$ containing the coherence factor $C(\boldsymbol{k}_{\rm F},\boldsymbol{k}'_{\rm F})$. We also calculate the field-angle dependences of $\langle\langle F(\varepsilon,\boldsymbol{k}_{\rm F},\boldsymbol{k}'_{\rm F})\rangle_{\rm FS'}\rangle_{\rm FS}$, which does not contain the coherence factor. When $\boldsymbol{H}$ is parallel to the node direction, $\langle\langle C(\boldsymbol{k}_{\rm F},\boldsymbol{k}'_{\rm F})D(\boldsymbol{k}_{\rm F},\boldsymbol{k}'_{\rm F})\rangle_{\rm FS'}\rangle_{\rm FS}$ shows the sharp maximum. On the other hand, $\langle\langle F(\varepsilon,\boldsymbol{k}_{\rm F},\boldsymbol{k}'_{\rm F})\rangle_{\rm FS'}\rangle_{\rm FS}$ shows the little field-angle dependence. This sharp maximum reproduces the behavior of $\Gamma(\alpha_{\rm M})$ in d-wave case [11].

The other contibution to $\rho_{\rm f}$ is $\omega_0(\boldsymbol{k}_{\rm F})$. When $\Gamma(\varepsilon,\boldsymbol{k}_{\rm F})$ =const., the field angle dependence of $\omega_0(\boldsymbol{k}_{\rm F})$ for a spheroidal FS is qualitatively not different from that for a isotropic FS [6]. When $\omega_0(\boldsymbol{k}_{\rm F})$ =const., $\rho_{\rm f}(T)\propto\Gamma(\varepsilon=k_{\rm B}T)$. In the d-wave case, the dependence of $\omega_0(\boldsymbol{k}_{\rm F})$ on the field-angle makes the behavior of $\Gamma(\alpha_{\rm M})$ stand out. As a result, $\rho_{\rm f}(\alpha_{\rm M})$ has a sharp maximum when $\boldsymbol{H}$ || the gap-node direction. On the other hand, in the s-wave case, the field angle dependence of $\omega_0(\boldsymbol{k}_{\rm F})$ makes the oscillation amplitude of $\Gamma(\alpha_{\rm M})$ inverted and $\rho_{\rm f}(\alpha_{\rm M})$ has its broad maximum when $\boldsymbol{H}$|| the gap-node direction.

At last, we comment on the experimental condition for measuring the flux-flow resistivity under rotating magnetic field. Our theory is based on the vortex bound states formed inside a vortex core. Therefore, extremely two dimensional system ,in which a Josephson vortex is formed parallel to the layer, is beyond our theoretical framework. In layered organic compounds κ-$(ET)_2Cu(NCS)_2$, in-plane field angular dependence of the Josephson-vortex flow resistance has already measured by Yasuzuka *et al.* [13], but in three dimensional system, the measurement of the flux-flow resistivity has not performed yet. We calculate $\rho_{\rm f}(\alpha_{\rm M})$ also in the case of the in-plane anisotropic FS [14]. In this case, the behavior of $\rho_{\rm f}(\alpha_{\rm M})$ is not qualitatively different from that in the isotropic FS case.

In conclusion, we theoretically studied in-plane magnetic field-angle dependence of the flux-flow resistivity for an uniaxially anisotropic FS. We show that the measurement of the flux-flow resistivity changing the field direction within the $a-b$ plane can detect both the position of gap nodes and the sign change of pairing potential.

The authors thank T. Okada and S. Yasuzuka for helpful discussions.

[1] T. Sakakibara, A. Yamada, J. Custers, K. Yano, T. Tayama, H. Aoki, and K. Machida, J. Phys. Soc. Jpn. **76**, 051004 (2007); Y. Matsuda, K. Izawa and I. Vekhter, J. Phys.: Condens. Matter **18**, R705 (2006).

[2] C. C. Tsuei and J. R. Kirtley, Rev. Mod. Phys. **72**, 969 (2000).

[3] T. Hanaguri, S. Nittaka, K. Kuroki, and H. Takagi, Science **328**, 474 (2010).

[4] N. B. Kopnin, G. E. Volovik, Phys. Rev. Lett. **79** (1997) 1377; Yu. G. Makhlin, Phys. Rev. B **56** (1997) 11872; N. B. Kopnin, G. E. Volovik, and Ü. Parts, Europhys. Lett. **32** 651 (1995); Alan T. Dorsey, Phys. Rev. B **46**, 8376 (1992).

[5] Y. Kato, J. Phys. Soc. Jpn. **69** (2000) 3378.

[6] Y. Higashi, Y. Nagai, M. Machida, N. Hayashi, J. Phys: Conf. Ser. **400**, 022025 (2012).

[7] G. E. Volovik, Pis'ma Zh. Eksp. Teor. Fiz. **70**, 601 (1999) [JETP Lett. **70**, 609 (1999)]; N. B. Kopnin and G. E. Volovik, Pis'ma Zh. Eksp. Teor. Fiz. **64**, 641 (1996) [JETP Lett. **64**, 690 (1996)].

[8] Y. Nagai, and N. Hayashi, Phys. Rev. Lett. **101** (2008) 097001; Y. Nagai, Y. Ueno, Y. Kato, and N. Hayashi, J. Phys. Soc. Jpn. **75** (2006) 104701, and references therein.

[9] Y. Nagai, Y. Kato, Phys. Rev. B **82** (2010) 174507.

[10] L. J. Buchholtz and G. Zwicknagl, Phys. Rev. B **23**, 5788 (1981); E. V. Thuneberg, J. Kurkijärvi, and D. Rainer, Phys. Rev. B **29**, 3913 (1984); N. Hayashi, Y. Kato, and M. Sigrist, J. Low Temp. Phys. **139**, 79 (2005).

[11] Y. Higashi, Y. Nagai, M. Machida, N. Hayashi, Physica C **471**, 828 (2011).

[12] Y. Higashi, Y. Nagai, M. Machida, N. Hayashi, Physica C **484**, 97 (2013).
[13] S. Yasuzuka, S. Uji, H. Satsukawa, M. Kimata, T. Terashima, H. Koga, Y. Yamamura, K. Saito, H. Akutsu, J. Yamada, Physica B **405**, S288 (2010).
[14] Y. Higashi, Y. Nagai, M. Machida, N. Hayashi, arXiv:cond-mat/1304.3164 (unpublished).